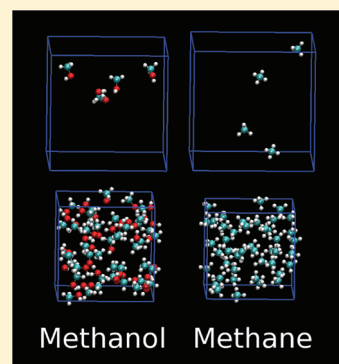


Vapor–Liquid Coexistence Curves for Methanol and Methane Using Dispersion-Corrected Density Functional Theory

Matthew J. McGrath,^{*,†,‡} I.-F. Will Kuo,[‡] Julius N. Ghogomu,^{¶,§} Christopher J. Mundy,^{||} and J. Ilja Siepmann[§][†]Department of Physics, University of Helsinki, P.O. Box 64, FI-00014 Helsinki, Finland[‡]Physical and Life Sciences Directorate, Lawrence Livermore National Laboratory, California 94550, United States[¶]Department of Chemistry, University of Dschang, B.P. 67, Dschang, Cameroon[§]Departments of Chemistry and Chemical Engineering and Materials Science and Chemical Theory Center, University of Minnesota, Minneapolis, Minnesota 55455, United States^{||}Chemical and Materials Sciences Division, Pacific Northwest National Laboratory, P.O. Box 999, Washington 99352, United States Supporting Information

ABSTRACT: First principles Monte Carlo simulations in the Gibbs and isobaric–isothermal ensembles were performed to map the vapor–liquid coexistence curves of methanol and methane described by Kohn–Sham density functional theory using the Becke–Lee–Yang–Parr (BLYP) exchange and correlation functionals with the Grimme correction term for dispersive (D2) interactions. The simulations indicate that the BLYP-D2 description with the TZV2P basis set underpredicts the saturated vapor densities and overpredicts the saturated liquid densities and critical and boiling temperatures for both compounds. Although the deviations are quite large, these results present a significant improvement over the BLYP functional without the correction term, which misses the experimental results by a larger extent in the opposite direction. Simulations at one temperature indicate that use of the larger QZV3P basis set may lead to improved saturated vapor densities, but not to significant changes in the liquid density.



■ INTRODUCTION

Knowledge of phase diagrams is essential to determine thermodynamic stability and to design separation processes. Particle-based simulation methods are routinely used to predict phase equilibria using empirical force fields, and the resulting phase diagrams provide rigorous tests of the accuracy of the underlying models. Enabled by advances in simulation algorithms and computational power, predictions of the vapor–liquid coexistence curves (VLCCs) have recently emerged for molecular systems^{1,2} where the interactions are described by first principles electronic structure calculations at the level of Kohn–Sham density functional theory (KS-DFT).³ Water was the topic of these initial first-principles predictions of vapor–liquid equilibria (VLE) because of its importance for biology, chemistry, and geology and also because its cohesive interactions are dominated by first-order electrostatic and polarization contributions that are well described by KS-DFT. In this paper, we present first principles simulations for methanol and methane, the smallest alcohol and alkane. Dispersive interactions make a very substantial contribution to the cohesive interactions of methanol and dominate those of methane; that is, these compounds pose a significantly greater challenge for electronic structure methods than water.

In the liquid phase of methanol, each molecule is, on average, involved in slightly less than two hydrogen bonds, and small cyclic and linear hydrogen-bonded clusters are prevalent⁴

compared with the extensive network of tetrahedrally connected molecules found in liquid water. Molecular simulations using first-principles interaction potentials have been performed for both bulk liquid methanol and the liquid–vapor interface at near-ambient conditions.^{5–8} In contrast, molecular simulations of methane described by electronic structure theory appear to be limited to high pressures and temperatures,^{9–11} where dispersive interactions play only a minor role.

First principles simulations usually employ KS-DFT with the local density approximation or generalized gradient approximation because good scaling with system size can be achieved with pure functionals. At this level, however, KS-DFT is known to poorly describe long-range dispersive interactions. Several methods have been developed to overcome this limitation, including parametrization of existing potentials, development of nonlocal functionals, atom-centered one-electron potentials, and empirical atom–atom correction terms. A comprehensive review of these methods is given by Grimme.¹² The empirically corrected functionals are promising (showing significant improvements over standard density functionals for many systems^{13–15} while also being straightforward to implement); of these, DFT-D2¹³ may be the most popular. First principles simulations with

Received: May 31, 2011

Revised: August 7, 2011

Published: August 10, 2011

empirical dispersive corrections have been carried out for water^{16–20} and carbon dioxide.²¹ Although simulations of water at ambient conditions show promising agreement with experiment for several properties,^{16–19} higher temperature data are not as promising.²⁰ Most of these studies carried out molecular dynamics simulations to obtain structural information of the pure liquid or the vapor–liquid interface.^{16,17,19–22} The notable exceptions are those of Weber and Asthagiri,¹⁸ who used hybrid Monte Carlo at fixed density to compute the free energy of hydration of water for several functionals near room temperature.

SIMULATION DETAILS

The purpose of this current study is to assess the accuracy of KS-DFT using the Becke–Lee–Yang–Parr (BLYP) exchange and correlation functionals^{23,24} and the Grimme dispersive (D2) correction¹³ for the prediction of the VLCCs of methanol and methane, for which dispersive interactions are much more significant than for water. All simulations were carried out with the CP2K simulation package, which includes Monte Carlo routines natively and computes the interaction energies of first principles system using the Quickstep module.²⁵ The VLE simulations were carried in the Gibbs ensemble²⁶ for a system size of 48 molecules at four temperatures for methane (120–180 K, in increments of 20 K) and five for methanol (350–550 K, in increments of 50 K). In addition, two lower temperatures for methanol (250 and 300 K) and one temperature for methane (100 K) were run in the isobaric–isothermal ensemble²⁷ to extend the liquid branch to lower temperatures ($p = 1$ bar). For all simulations with the BLYP-D2 representation, a cutoff at 40 Å was used for the dispersion correction. Most of the simulations used the popular TZV2P basis set²⁵ with an auxiliary basis plane wave cutoff of 600 Ry. As an additional test, a larger basis set (QZV3P, using both 600 and 1200 Ry cutoffs) was also employed for three temperatures in this work: 300 and 450 K for methanol, and 160 K for methane.

Given the relatively small number of molecules in the system, it is important to assess the impact of the system size on the critical and normal boiling points. A previous study by this group demonstrated that as long as long-range interactions are properly treated (analytical tail corrections for Lennard-Jones interactions and Ewald summation for Coulomb interactions), 32 water molecules yield VLCC data differing by much less than the statistical uncertainty of first principles simulations from those of a 512-molecule system.¹ However, given the different balances of dispersive and electrostatic interactions for methane and methanol, additional simulations were carried out to probe the issue further. Using standard simulation protocols and the TraPPE–UA force field,²⁸ the critical and normal boiling temperatures of methane for a system consisting of 48 molecules were computed to be 198 ± 2 K and 114 ± 1 K, respectively. These values compare well to 191.4 ± 1.3 and 111.5 ± 0.9 K, respectively, obtained for a 400-molecule system.²⁸

For the 48-molecule methanol system represented by the TraPPE–UA force field,²⁹ fluctuations in the cell volume prevented using a reduced temperature higher than ≈ 0.9 . The range of applicability of the scaling law is more limited for polar molecules, and we followed the procedure outlined by Chen et al.²⁹ to estimate an effective critical exponent that somewhat corrects for the absence of simulation data very close to the critical point. The resulting critical temperature for the 48-molecule

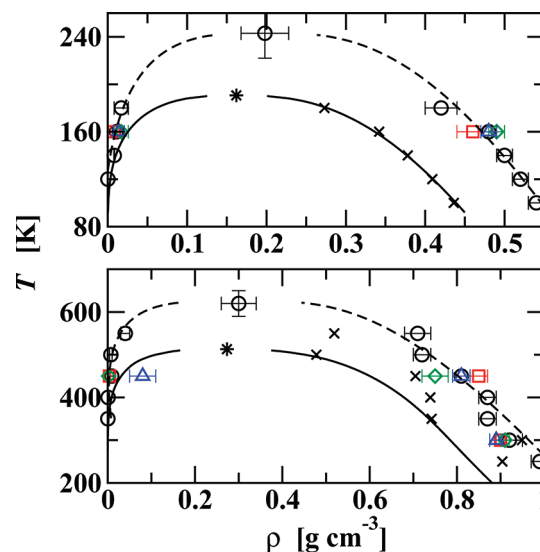


Figure 1. Vapor–liquid coexistence curves for methane (top) and methanol (bottom). The solid lines and stars represent the experimental data.^{38,39} The black circles, red squares, green diamonds, and blue triangles represent simulation data for the BLYP-D2 representation with the basis set–cutoff combinations TZV2P-600, TZV2P-1200, QZV3P-600, and QZV3P-1200, respectively. The dashed lines indicate scaling law fits to the TZV2P-600 data. The crosses indicate the initial density for the TZV2P-600 simulations. The uncertainties on the experimental critical points are smaller than the symbols.

system is 515 ± 5 K, compared with 502 ± 2 K obtained for a 500-molecule system and the TraPPE–UA force field.²⁹ This difference is less than the statistical uncertainty of the current first-principles Monte Carlo simulations. The uncertainty estimate of the critical point for methanol for BLYP-D2 includes the statistical uncertainty and contributions arising from the estimation of finite-size effects and the effective critical exponent. The normal boiling temperatures obtained for the 48- and 500-molecule simulations with the TraPPE–UA force field are 338 ± 2 and 340 ± 1 K, respectively.

To increase the sampling efficiency of the first principles Monte Carlo simulations, presampling sequences with an approximate potential were incorporated for translations, rotations, and configurational-bias particle exchanges.^{30–33} This required finding a simple analytical potential function that can satisfactorily reproduce the energy differences between various configurations as calculated with the more expensive BLYP-D2 representation. The fitting procedure was identical to that followed for simulations of gaseous hydrogen fluoride³⁴ and involved simple potentials with atom-centered six- and five-site models for methanol and methane, respectively. The resulting parameters are listed in the Supporting Information. Move probabilities and maximum displacements were adjusted as in previous works.^{1,35,36} The simulations were run for ~ 600 Monte Carlo cycles (where one cycle consists of $N = 48$ moves with the acceptance based on the BLYP-D2 energies, i.e., an entire presampling sequence counts as a single move). The equilibration periods took about 100–300 cycles, with the remainder of the runs used for the calculation of the ensemble averages. The coexistence data were obtained from the two peaks in density histograms, and the uncertainties were estimated from the full width at half-maximum (fwhm) of these peaks.

RESULTS AND DISCUSSION

The computed VLCCs for both methane and methanol are depicted in Figure 1. The BLYP-D2 level of electronic structure theory yields two-phase coexistence for methane and methanol for the whole temperature ranges explored here. This is a significant improvement over BLYP without dispersion corrections for which exploratory attempts failed to find coexistence for methanol at 250 and 300 K. [We did not even try BLYP for methane because it does not produce a bound state for the dimer.³⁷] Although the results for BLYP-D2 are a step forward, this representation yields liquid densities that are overestimated by ~ 15 – 20% at low reduced temperatures. Here, it should be noted that all but one of the simulations (the exception being methanol at 300 K) were initiated from lower densities, and the liquid phases became more dense during the equilibration periods. Extrapolation of the VLCC data for BLYP-D2/TZV2P-600 yields critical temperatures of 240 ± 20 and 620 ± 30 K for methane and methanol, respectively, and critical densities of 0.20 ± 0.03 and 0.30 ± 0.04 g cm⁻³, respectively; T_c and ρ_c are overestimated by ≈ 25 and 10% , respectively, compared with the experimental values.^{38,39}

The overestimation found for the saturated liquid densities and the critical temperatures points to BLYP-D2 favoring the condensed phase by too great an extent compared with the vapor phase. The overbinding of BLYP-D2/TZV2P-600 noticed here for methane and methanol agrees with preliminary high-temperature Gibbs ensemble Monte Carlo simulations of water that also indicate an overestimation of the saturated liquid density and of the Gibbs free energy of transfer.²⁰ Similarly, Weber and Asthagiri¹⁸ found that temperature elevation at fixed density is required to improve the structure and hydration free energy of water described by BLYP-D2. A previous study of the VLCC of water using pure functionals indicated that increasing the size of the basis set used in the calculation results in a less dense liquid phase for BLYP,² whereas the simulations with the D2 corrections do not yield substantial shifts in the liquid densities when the basis set or cutoff are increased (see Figure 1). Judging from the fact that the VLCCs for BLYP-D2/TZV2P-600 appear to be shifted upward by a nearly constant amount, it appears likely that these deficiencies are caused by the functional/correction term and not by the neglect of nuclear quantum effects, which decrease in importance with increasing temperature. However, it should be emphasized that inclusion of nuclear quantum effects would shift the predicted saturated liquid densities closer to the experimental data. For example, Balog et al.⁴⁰ observed a 6% decrease in the liquid density of methane due to nuclear quantum effects from path-integral simulations using an empirical force field.

The saturated vapor pressures are not directly available from our first principles Monte Carlo simulations, and we used the ideal gas law to estimate the vapor pressures from the corresponding densities (an approximation that holds well at low reduced temperatures). As judged from Clausius–Clapeyron plots (see Figure 2), the BLYP-D2/TZV2P-600 description yields saturated vapor pressures that fall very significantly below the experimental data and normal boiling points of 143 ± 2 and 405 ± 9 K for methane and methanol, respectively, which are overestimated by ≈ 30 and 20% . The vapor phase for one methanol run, BLYP-D2/QZV3P-1200 at 450 K, is quite dense, and structural analysis reveals the presence of dimers and trimers (preventing the use of the ideal gas approximation), although these clusters are seldom long-lived. The slopes of the Clausius–Clapeyron plots yield heats of vaporization of 19 ± 2 and

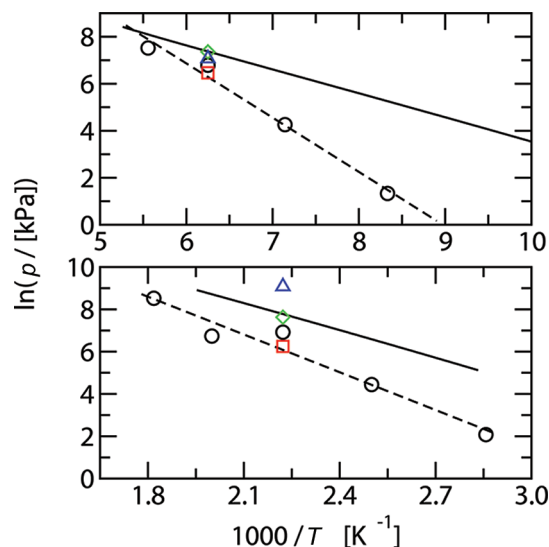


Figure 2. Clausius–Clapeyron plots of methane (top) and methanol (bottom). The solid lines represent the experimental data.^{38,39} The symbols depict the BLYP-D2 simulation data with colors and symbol types as in Figure 1. The dashed lines show linear fits of the TZV2P-600 data.

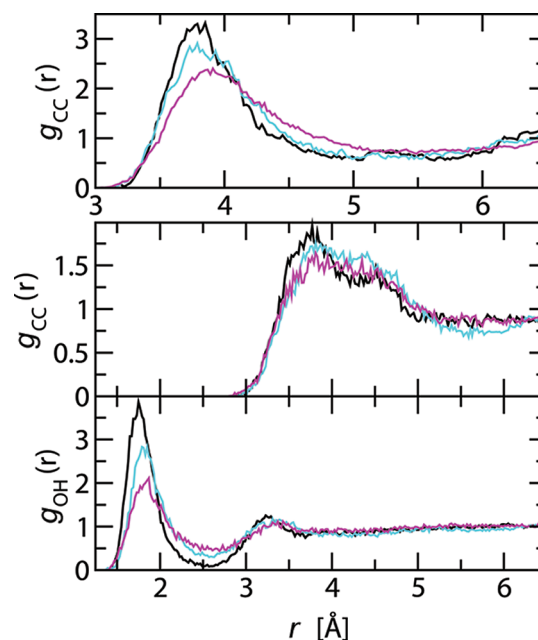


Figure 3. Selected liquid-phase radial distribution functions. The black, cyan, and magenta lines show (top) the C–C RDF for methane at $T = 100$, 140 , and 180 K, respectively; (middle) the C–C RDF for methanol at $T = 350$, 450 , and 550 K, respectively; and (bottom) the O–H RDF for methanol at the same three temperatures. The bin width is 0.02 Å.

39 ± 9 kJ mol⁻¹ for methane and methanol, respectively. The former value exceeds the experimental value at the normal boiling point by a factor of about 2, whereas the latter value is only slightly larger than its experimental counterpart. Thus, the upward shift of the VLCC of methane for BLYP-D2/TZV2P-600 is likely caused by the very significant overestimation of the heat of vaporization, whereas both enthalpic and entropic factors

must contribute for methanol. For the saturated vapor densities/pressures, use of the larger QZV3P basis set leads to increased values that are closer to experiment (again, use of the ideal gas law leads to an overestimation of the pressure for the TZV3P-1200 due to extensive clustering).

Selected liquid-phase radial distribution functions (RDFs) for both compounds at three temperatures are shown in Figure 3. The C–C RDF of methane exhibits the structure typical for a nonpolar compound with a (nearly) spherically symmetric interaction potential. The first peak shifts outward and its height decreases substantially with increasing temperature. However, the number of molecules in the first solvation shell remains close to 11 at all three temperatures. In comparison, the C–C RDF for the methyl group of methanol indicates more disorder (as judged from the smaller height of the first peak and the less pronounced first minimum) and a coordination number of only 8.5–10 for the first solvation shell. The O–H RDF for methanol shows features typical for a system with pronounced hydrogen bonding; that is, the first peak is very sharp and located at a short separation of $r = 1.8$ Å that does not shift significantly with increasing temperature. However, the value of the number integral at $r = 2.6$ Å decreases from 2.0 to 1.8 as the temperature is increased from 350 to 550 K; that is, the extent of hydrogen bonding decreases.

CONCLUSIONS

We have presented here the first calculations of the vapor–liquid coexistence curves for molecular systems using dispersion-corrected density functional theory. Using the dispersion correction of Grimme¹³ and the BLYP density functional^{23,24} with the TZV2P basis set,²⁵ methane and methanol were found to be overbound, resulting in VLCCs that are shifted upward; that is, the saturated liquid densities and critical temperatures are too high, whereas the vapor densities are too low. With the D2 correction, there appears to be less sensitivity (particularly for the liquid branch) to the basis set and the plane-wave cutoff than for the pure functional, but use of the larger QZV3P basis set yields improved vapor densities/pressures. Although the dispersion-corrected functionals do not yet yield quantitative accuracy, they present a tremendous improvement for systems with a significant contribution to the cohesive energy from dispersive interactions.

ASSOCIATED CONTENT

S Supporting Information. Numerical data for the predicted VLCC for methane and methanol and a detailed description of the approximate potentials are provided in the Supporting Information. This material is available free of charge via the Internet at <http://pubs.acs.org/>.

AUTHOR INFORMATION

Corresponding Author

*E-mail: mcgrath@theory.biophys.kyoto-u.ac.jp.

Present Addresses

[†]Department of Biophysics, Graduate School of Science, Kyoto University, Sakyo Kyoto 606-8502, Japan

ACKNOWLEDGMENT

Financial support from the National Science Foundation (CBET-0756641 and OISE-0853294), the European Research

Council (StG 257360-MOCAPAF), and a Fulbright Senior Scholar Award to J.N.G. (enabling an extended visit to the University of Minnesota) is gratefully acknowledged. Part of this research was performed under the auspices of the U.S. Department of Energy by Lawrence Livermore National Laboratory under Contract DE-AC52-07NA27344 with computing support from the M&IC Program and an Institutional Grand Challenge Award and by the Division of Chemical Sciences, Geosciences, and Biosciences, Office of Basic Energy Sciences under Contract DE-AC06-76RLO1830 with Battelle Memorial Institute, which operates the Pacific Northwest National Laboratory, a multi-program national laboratory. Part of the simulations used resources provided by the Minnesota Supercomputing Institute. Xmgrace, VMD, and GIMP were used in preparation of the figures.

REFERENCES

- (1) McGrath, M. J.; Siepmann, J. I.; Kuo, I.-F. W.; Mundy, C. J.; VandeVondele, J.; Hutter, J.; Mohamed, F.; Krack, M. *J. Phys. Chem. A* **2006**, *110*, 640–646.
- (2) McGrath, M. J.; Siepmann, J. I.; Kuo, I.-F. W.; Mundy, C. J. *Mol. Phys.* **2006**, *104*, 3619–3626.
- (3) Kohn, W.; Sham, L. J. *Phys. Rev.* **1965**, *140*, A1133–A1138.
- (4) Kashtanov, S.; Augustson, A.; Rubensson, J.-E.; Nordgren, J.; Ågren, A.; Guo, J.-H.; Luo, Y. *Phys. Rev. B* **2005**, *71*, 104205.
- (5) Tsuchida, E.; Kanada, Y.; Tsukada, M. *Chem. Phys. Lett.* **1999**, *311*, 236–240.
- (6) Morrone, J. A.; Tuckerman, M. E. *J. Chem. Phys.* **2002**, *117*, 4403–4413.
- (7) Handgraaf, J.-W.; Meijer, E. J.; Gaigeot, M.-P. *J. Chem. Phys.* **2004**, *121*, 10111–10119.
- (8) Kuo, I.-F. W.; Mundy, C. J.; McGrath, M. J.; Siepmann, J. I. *J. Phys. Chem. C* **2008**, *112*, 15412–15418.
- (9) Ancilotto, F.; Chiarotti, G. L.; Scandolo, S.; Tosatti, E. *Science* **1997**, *275*, 1288–1290.
- (10) Kress, J. D.; Bickham, S. R.; Collins, L. A.; Holian, B. L.; Goedecker, S. *Phys. Rev. Lett.* **1999**, *83*, 3896–3899.
- (11) Goldman, N.; Reed, E. J.; Fried, L. E. *J. Chem. Phys.* **2009**, *131*, 204103.
- (12) Grimme, S. *Wiley Inter. Rev.: Comp. Mol. Sci.* **2011**, *1*, 211–228.
- (13) Grimme, S. *J. Comput. Chem.* **2006**, *27*, 1787–1799.
- (14) Antony, J.; Grimme, S. *Phys. Chem. Chem. Phys.* **2006**, *8*, 5287–5293.
- (15) Peverati, R.; Baldrige, K. K. *J. Chem. Theory Comput.* **2008**, *4*, 2030–2048.
- (16) Schmidt, J.; VandeVondele, J.; Kuo, I.-F. W.; Sebastiani, D.; Siepmann, J. I.; Hutter, J.; Mundy, C. J. *J. Phys. Chem. B* **2009**, *113*, 11959–11964.
- (17) Lin, I.-C.; Seitsonen, A. P.; Coutinho-Neto, M. D.; Tavernelli, I.; Rothlisberger, U. *J. Phys. Chem. B* **2009**, *113*, 1127–1131.
- (18) Weber, V.; Asthagiri, D. *J. Chem. Phys.* **2010**, *133*, 141101.
- (19) Kühne, T. D.; Pascal, T. A.; Kaxiras, E.; Jung, Y. *J. Phys. Chem. Lett.* **2011**, *2*, 105–113.
- (20) Baer, M. D.; Mundy, C. J.; McGrath, M. J.; Kuo, I.-F. W.; Siepmann, J. I.; Tobias, D. *J. Chem. Phys.* in press.
- (21) Balasubramanian, S.; Kohlmeyer, A.; Klein, M. L. *J. Chem. Phys.* **2009**, *131*, 144506.
- (22) Murdachaew, G.; Mundy, C. J.; Schenter, G. K. *J. Chem. Phys.* **2010**, *132*, 164102.
- (23) Becke, A. D. *Phys. Rev. A* **1988**, *38*, 3098–3100.
- (24) Lee, C.; Yang, W.; Parr, R. G. *Phys. Rev. B* **1988**, *37*, 785–789.
- (25) VandeVondele, J.; Krack, M.; Mohamed, F.; Parrinello, M.; Chassaing, T.; Hutter, J. *Comput. Phys. Commun.* **2005**, *167*, 103–128.
- (26) Panagiotopoulos, A. Z. *Mol. Phys.* **1987**, *61*, 813–826.
- (27) McDonald, I. R. *Mol. Phys.* **1972**, *23*, 41–58.

- (28) Martin, M. G.; Siepmann, J. I. *J. Phys. Chem. B* **1998**, *102*, 2569–2577.
- (29) Chen, B.; Potoff, J. J.; Siepmann, J. I. *J. Phys. Chem. B* **2001**, *105*, 3093–3104.
- (30) Iftimie, R.; Salahub, D.; Wei, D.; Schofield, J. *J. Chem. Phys.* **2000**, *113*, 4852–4862.
- (31) Gelb, L. D. *J. Chem. Phys.* **2003**, *118*, 7747–7750.
- (32) Siepmann, J. I.; Frenkel, D. *Mol. Phys.* **1992**, *75*, 59–70.
- (33) Smit, B.; Karaborni, S.; Siepmann, J. I. *J. Chem. Phys.* **1995**, *102*, 2126–2140.
- (34) McGrath, M. J.; Ghogomu, J. N.; Mundy, C. J.; Kuo, I.-F. W.; Siepmann, J. I. *J. Phys. Chem. Chem. Phys.* **2010**, *12*, 7678–7687.
- (35) Kuo, I.-F. W.; Mundy, C. J.; McGrath, M. J.; Siepmann, J. I.; VandeVondele, J.; Sprik, M.; Hutter, J.; Chen, B.; Klein, M. L.; Mohamed, F.; Krack, M.; Parrinello, M. *J. Phys. Chem. B* **2004**, *108*, 12990–12998.
- (36) McGrath, M. J.; Siepmann, J. I.; Kuo, I.-F. W.; Mundy, C. J.; VandeVondele, J.; Hutter, J.; Mohamed, F.; Krack, M. *ChemPhysChem* **2005**, *6*, 1894–1901.
- (37) Tsuzuki, S.; Lüthi, H. P. *J. Chem. Phys.* **2001**, *114*, 3949–3957.
- (38) Smith, B. D.; Srivastava, R. *Thermodynamic Data for Pure Compounds: Part A, Hydrocarbons and Ketones*; Elsevier: Amsterdam, 1986.
- (39) Smith, B. D.; Srivastava, R. *Thermodynamic Data for Pure Compounds: Part B, Halogenated Hydrocarbons and Alcohols*; Elsevier: Amsterdam, 1986.
- (40) Balog, E.; Hughes, A. L.; Martyna, G. J. *J. Chem. Phys.* **2000**, *112*, 870–880.